nature
structural biology

Control of tetrapyrrole biosynthesis by alternate quaternary forms of porphobilinogen synthase

Sabine Breinig[1], Jukka Kervinen[2], Linda Stith[1], Andrew S Wasson[3], Robert Fairman[3], Alexander Wlodawer[4], Alexander Zdanov[4] & Eileen K Jaffe[1]

Porphobilinogen synthase (PBGS) catalyzes the first common step in the biosynthesis of tetrapyrroles (such as heme and chlorophyll). Although the predominant oligomeric form of this enzyme, as inferred from many crystal structures, is that of a homo-octamer, a rare human PBGS allele, F12L, reveals the presence of a hexameric form. Rearrangement of an N-terminal arm is responsible for this oligomeric switch, which results in profound changes in kinetic behavior. The structural transition between octamer and hexamer must proceed through an unparalleled equilibrium containing two different dimer structures. The allosteric magnesium, present in most PBGS, has a binding site in the octamer but not in the hexamer. The unprecedented structural rearrangement reported here relates to the allosteric regulation of PBGS and suggests that alternative PBGS oligomers may function in a magnesium-dependent regulation of tetrapyrrole biosynthesis in plants and some bacteria.

The enzyme porphobilinogen synthase (PBGS), also known as 5-aminolevulinic acid dehydratase (ALAD), is an ancient and highly conserved protein that catalyzes the first common step in the biosynthesis of tetrapyrroles including heme, chlorophyll, vitamin B_{12} and cofactor F_{430} (refs. 1,2). Human PBGS variant F12L is an example of natural biological variation that provides considerable insight into structure-function relationships in PBGS. This rare human allele was first discovered in a routine neonatal screen for hereditary tyrosinemia[3]. Succinyl acetone, a metabolic byproduct of enzyme dysfunction in hereditary tyrosinemia, is a potent inhibitor of PBGS; hence, PBGS activity in neonatal blood is used as a screening tool for this disease[4]. In the cited case, the asymptomatic infant did not have hereditary tyrosinemia but was instead a heterozygote of the F12L variant and normal PBGS, with enzymatic activity ~12% of normal[3]. When the F12L variant was expressed in CHO cells, or fused with GST and expressed in bacteria, the mutant protein was found to be virtually inactive[3,5]. Because human PBGS is an octamer that shows half-of-the-sites reactivity (PDB entry 1E51)[6,7], we found the 12% (or 1/8 rather than 1/2 or 1/4) activity of the heteromeric wild-type–F12L PBGS to be intriguing and undertook study of the F12L variant. We show here that the F12L variant has profoundly different kinetic properties from wild-type human PBGS and that the properties of the F12L variant arise from a markedly altered quaternary structure.

RESULTS

The properties of human PBGS variant F12L

Human PBGS variant F12L is notably different from the wild-type protein. Characterization of the purified F12L variant confirmed that the catalytic activity is very low under conditions at which wild-type human PBGS is most active. However, the F12L variant exhibits a remarkably altered pH-rate profile and shows considerable activity at basic pH values (**Fig. 1a**). The K_m and V_{max} values of the F12L variant and wild-type human PBGS were determined at pH 7, which is optimal for the wild-type protein, and at pH 9, which is optimal for the F12L variant (**Table 1**). The F12L variant exhibits normal Michaelis-Menten kinetics with extraordinarily high K_m values, well above physiological concentrations of the substrate 5-aminolevulinic acid (ALA). However, at pH 9 the V_{max} of the F12L variant is substantially higher than that of the wild-type protein. Under conditions of optimal pH and in the presence of an optimal configuration of metal ions, wild-type PBGS from all characterized species are reported to have K_m values in the range of 100 μM (refs. 6,8–10), as is seen here for wild-type human PBGS at pH 7. The kinetic behavior of wild-type human PBGS at pH 9 did not exhibit standard Michaelis-Menten kinetics, the basis of which was not at first apparent (see below). On cursory examination, the wild-type protein seemed to exhibit an extreme negative cooperativity with a Hill coefficient on the order of 0.35.

Further evidence for differences between the F12L variant and the wild-type protein came from variations in mobility during anion-exchange chromatography (**Fig. 1b**) and during native gel electrophoresis (**Fig. 1c**), both of which suggest a difference in oligomeric structure. Separation on an anion-exchange column generally reflects a different surface charge, which cannot be due to the replacement of neutral leucine for neutral phenylalanine. Separation of two species with identical charge/mass ratio by electrophoresis indicates either a different size or a different shape. Together, these differences suggested

[1]Fox Chase Cancer Center, 333 Cottman Avenue, Philadelphia, Pennsylvania 19111-2497, USA. [2]3-Dimensional Pharmaceuticals, Inc., 665 Stockton Drive, Exton, Pennsylvania 19341, USA. [3]Department of Biology, Haverford College, 370 Lancaster Avenue, Haverford, Pennsylvania 19041, USA. [4]Macromolecular Crystallography Laboratory, NCI-Frederick, Frederick, Maryland 21702, USA. Correspondence should be addressed to E.K.J. (ek_jaffe@fccc.edu).

Published online 3 August 2003; doi:10.1038/nsb963

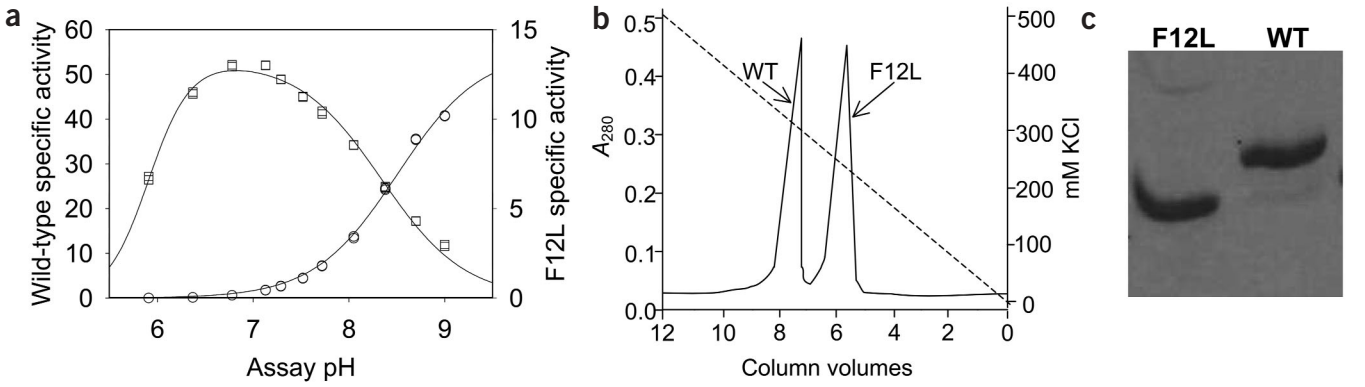

Figure 1 Characteristics of wild-type human PBGS relative to the F12L variant. (**a**) The pH-rate profile for human PBGS (□) exhibits a two-proton activating pK_a of 5.9 and a one-proton deactivating pK_b of 8.3. In contrast, the F12L variant (○) shows a single one-proton activating pK_a of 8.5. (**b**) The chromatographic separation of wild-type human (WT) PBGS and the F12L variant on a mono-Q column. (**c**) The differential mobility of wild-type (WT) human PBGS and the F12L variant on 12.5% (w/v) native PAGE.

that the F12L variant and wild-type human PBGS exist in different oligomeric states.

When the wild-type and mutant proteins were subjected to sedimentation equilibrium analysis using an analytical ultracentrifuge, the molecular masses of the wild-type protein and the F12L variant were found to be 244,000 ± 8,900 and 197,900 ± 6,500 Da, respectively (data not shown). The former value is midway between that expected for an octamer and a hexamer, whereas the latter is midway between that expected for a hexamer and a tetramer. In model analysis of the data, the wild-type protein fit best to a three-state model of dimer, hexamer and octamer at 7.6%, 51% and 42%, respectively, whereas the F12L variant fit best to a two-state model of tetramer and hexamer at a ratio of 70% to 30%, with octamer absent. Hence we undertook the determination of the crystal structure of human PBGS variant F12L.

A novel structural change for the F12L variant

Seventeen previously determined crystal structures of PBGS[11–20] from fungi, metazoa and bacteria reveal a common homo-octameric structure in which four dimers are related by a 90° rotation around a central axis (**Fig. 2a**). PBGS is a member of the aldolase superfamily of TIM α/β barrel proteins[21]. In each subunit the catalytic core resides completely within the barrel and an N-terminal arm of ≥20 residues is involved in extensive subunit interactions. The sequence of the catalytic core is phylogenetically conserved, but that of the N-terminal arm is not. The PBGS dimer seen in the octamer (**Fig. 2a**, left) involves highly conserved barrel-to-barrel contacts and the N-terminal arm of one subunit is hugging the barrel of the sister subunit. Hence, this has been referred to as the hugging dimer[2]. The side chain of amino acid 12 does not participate in the hugging interaction. Assembly of the tetramer (**Fig. 2a**, middle) adds an additional reciprocal interaction between the arm of one subunit and the base of an α/β barrel from a neighboring dimer. The side chain of amino acid 12 participates in this subunit interaction. Prior to the current determination of the crystal structure of the F12L variant, it was presumed that all PBGS proteins shared the same homo-octameric structure[2]. However, for PBGS from green plants and some bacteria, there is kinetic evidence suggesting that the maximally active octamer can dissociate into smaller, less active structural units[9,22].

Table 1 Kinetic parameters of homomeric and heteromeric human PBGS

		F12L	Wild type	WT+F12L Pool I	WT+F12L Pool II
K_{m1}	pH 7		0.25 ± 0.01	0.21 ± 0.01	0.13 ± 0.01
V_{max1}	pH 7		55.5 ± 0.2	2.37 ± 0.07	20.20 ± 0.99
K_{m2}	pH 7	17.7 ± 1.1		7.71 ± 0.72	4.85 ± 2.04
V_{max2}	pH 7	1.14 ± 0.05		4.78 ± 0.10	10.92 ± 0.85
K_{m1}	pH 9		0.35 ± 0.09	0.10 ± 0.13	0.024 ± 0.003
V_{max1}	pH 9		8.16 ± 0.13	0.32 ± 0.23	3.19 ± 0.15
K_{m2}	pH 9	4.6 ± 0.1	4.46 ± 0.80	3.74 ± 0.29	2.35 ± 0.21
V_{max2}	pH 9	18.2 ± 0.2	6.67 ± 0.36	12.16 ± 0.18	8.70 ± 0.17

Pool I and Pool II are the two pools of PBGS activity eluted from the Q-Sepharose column (**Fig. 3a**) after further purification on a Sephacryl S-300 column. K_{m1} and K_{m2} (both mM) are interpreted as the K_m values for the octamer and hexamer, respectively. The reported V_{max} values (μmol h^{-1} mg^{-1}) reflect the mole fraction of quaternary species under assay conditions, which remains to be determined. Fitted K_m values are independent of the distribution of quaternary species.

Notably, the newly determined crystal structure of the F12L human PBGS allele reveals a quaternary structure that involves considerable rearrangement of the N-terminal arm relative to the α/β barrel (**Fig. 2b**, PDB entry 1PV8). In this case, the dimer retains the aforementioned barrel-to-barrel contacts but the N-terminal arms are detached rather than hugging. In the oligomeric structure there are three detached dimers, each rotated 120° around a central axis to form a hexamer. The PBGS hexamer retains the relationship between the arm from one dimer, where Leu12 is located, and the base of the α/β barrel of a neighboring dimer. The subunit interface that involves the side chain of amino acid 12 is not the subunit interface that is most markedly affected by the F12L mutation. The unprecedented structural transition from the octamer observed for wild-type human PBGS to the hexamer observed for the F12L variant is an outstanding example of how a naturally occurring small mutational change can have a profound effect on the structure and function of a protein. From viewing these structures, it appears that any equilibration between octamer and hexamer most probably proceeds through the interconversion of the hugging dimer and the detached dimer.

The new structure of the F12L variant determined at 2.2-Å resolution contains regions of disorder that impede a structural comparison of the active site relative to the previously deposited wild-type human PBGS structure (PDB entry 1E51, 2.83-Å resolution). Nevertheless, it is clear that amino acid 12 does not interact directly with active-site residues in either structure. Furthermore, for those amino acids

observed in both structures, most are superimposable. Thus, to further probe the basis for the unusual kinetic properties of the F12L variant (see **Fig. 1**, **Table 1**), we undertook coexpression of the F12L variant and wild-type human PBGS.

Coexpression of wild type and the F12L variant

A coexpression system was prepared to produce both wild-type human PBGS and the F12L variant in a 1:1 ratio from the same RNA message. Purification of the coexpressed protein, called WT+F12L, was found to yield two distinct peaks of PBGS protein on anion exchange chromatography (**Fig. 3a**). The peak to elute first (pool I) runs comparably to the F12L variant on a native gel, whereas the second peak (pool II) runs comparably to wild-type human PBGS (**Fig. 3b**). Pool I showed enhanced activity at pH 9 and pool II showed enhanced activity at pH 7. Both pools were individually subjected to analysis by mass spectroscopy after a tryptic digest and each was found to contain substantial amounts of both the N-terminal 2,010.2 Da phenylalanine-containing peptide and the 1,976.2 Da leucine-containing peptide, confirming that both pools contain heteromeric species. The percentage of each chain in the heteromeric pools was quantified by N-terminal sequencing to show that pool I contains 48.5% phenylalanine and 51.5% leucine whereas pool II contains 71.1% phenylalanine and 28.3% leucine. These ratios do not obviously reveal what governs the quaternary structure of the heteromeric species. Pools I and II were further purified by gel filtration on Sephacryl S300, which reduced cross contamination of the heteromers. The pH-rate profiles of the S300 purified Pools I and II (**Fig. 3c**) are remarkably like the F12L variant and wild-type human PBGS, respectively. Based on the chromatographic, mass spectroscopy and quantitative N-terminal sequencing data, we conclude that pool I is comprised of hetero-hexamers and that pool II is comprised of hetero-octamers. The pH-rate profiles are found to be dominated more by the quaternary structure than by the amino acid composition at position 12.

The kinetic parameters K_m and V_{max} of the S300 purified pools were determined at pH 7 and at pH 9 (**Table 1**). The kinetic data do not follow a simple Michaelis-Menten relationship, but can be attributed to catalysis by two different forms of the enzyme that have different K_m and V_{max} values[23]. The kinetic data uniformly fit a model in which hexameric and octameric forms of the enzyme exhibit high and low K_m values, respectively (**Fig. 3d**). With the exception of the trace amount of octamer present for pool I that is detected at pH 9, all the kinetic values are well determined (**Table 1**). The octamer-hexamer model provided a superior fit to the data for wild-type human PBGS at pH 9 (**Table 1**). The factors that govern equilibration of human PBGS heteromers under assay conditions remain to be elucidated.

The data presented on wild-type human PBGS, the F12L variant and the WT+F12L heteromers definitively establish that the kinetic differences between the wild-type protein and the F12L variant are primarily due to the difference in quaternary structure. The thermodynamic basis for the unprecedented structural transition between octamer and hexamer of human PBGS remains unclear. The existence of heteromeric mixtures of octamer and hexamer formed during expression of WT+F12L indicates that discrimination between these two oligomers occurs during the folding and assembly process. How the F12L mutation alters the folding and assembly process to favor the hexamer over the octamer is an open question. The current data address the end products of folding and assembly, but not the process.

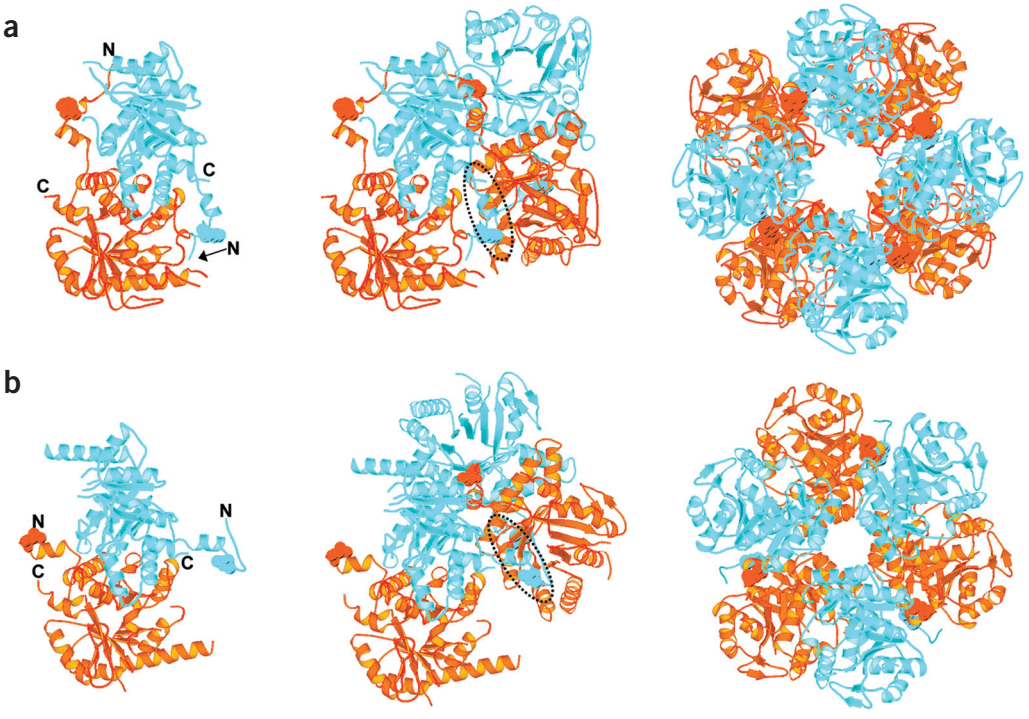

Figure 2 Comparison of newly determined structure of the hexameric human PBGS variant F12L (PDB entry 1PV8) with that of the human PBGS octamer (PDB entry 1E51). The N and C termini are labeled in the dimers as these structures contain regions of disorder that appear as breaks in the chains. (**a**) The crystallographic asymmetric unit of wild-type human PBGS (left) is a homodimer with subunits colored orange and cyan. In this hugging dimer, an N-terminal arm of each subunit is wrapped around the α/β barrel of the adjacent subunit. Phe12 is in space-filling representation. The assembly of a homo-tetramer (middle, orientation same as left) adds new reciprocal arm-to-barrel interactions (broken oval) between the cyan subunit of one dimer and the orange subunit of the adjacent dimer. The second hugging dimer is rotated 90° around a central axis. The octamer (right, viewed from above as a pinwheel) includes two additional dimers, each rotated 90° around the central axis closing the circular arrangement. (**b**) The crystallographic dimer of the F12L variant (left) shows the barrels oriented as in **a**, but the N-terminal arms do not hug the adjacent barrels (a detached dimer). Leu12 is in space-filling representation. Addition of a second detached dimer (middle, orientation same as left) involves the same reciprocal arm-to-barrel interaction (broken oval) as is seen to form in panel **a** between the cyan subunit of the first dimer and the orange subunit of the second dimer. However, the angle of rotation around the central axis is 120°. Addition of the third dimer (right, pinwheel representation, cyan subunits on top) completes the 360° rotation around the central axis.

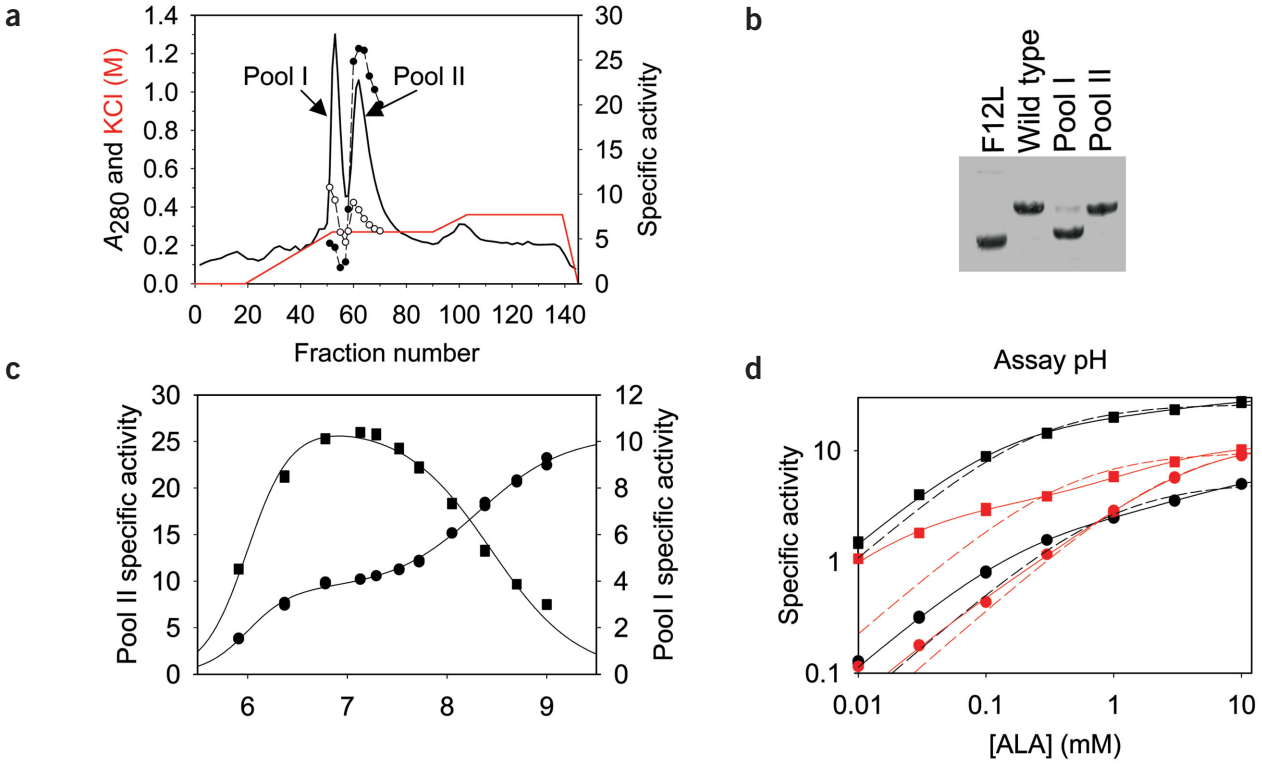

Figure 3 Characteristics of coexpressed WT+F12L. (**a**) Separation of two peaks of PBGS protein on Q-Sepharose; KCl gradient (red line), A_{280} (black line). Both pools showed PBGS activity at pH 7 (●) and at pH 9 (○). (**b**) The mobility of the two pools of WT+F12L relative to wild-type (WT) human PBGS and the F12L variant on native gel electrophoresis. (**c**) The pH-rate profiles for pool I (●) and pool II (■) after further purification on Sephacryl S300. (**d**) Determination of K_m and V_{max} values for the S300 purified pool I (●) and pool II (■) at pH 7 (black) and pH 9 (red). Dashed lines indicate the poor fits to standard hyperbolic saturation kinetics. Solid lines indicate the superior fit to a double hyperbola model where two forms of the enzyme are catalyzing the same reaction (see text and **Table 1**).

DISCUSSION

Octamer vs. hexamer pH optimum

In light of the structures of octameric vs. hexameric human PBGS, a hypothesis can be formulated concerning the marked difference in pH optima for these two forms of PBGS. The chemistry of the PBGS-catalyzed reaction requires the formation of at least two Schiff base intermediates[2,12,16,17,20]. Formation of the carbinolamine precursors to these Schiff bases requires that the participating amino groups are uncharged, or that the local pH is above the pK_a of the amino groups. One notable structural difference between hexameric and octameric PBGS is the degree of order found in the amino acids that comprise the active-site lid. The crystal structure of the hexameric PBGS F12L variant is lacking in density from most of the residues that make up the active site lid, thus implying that the hexamer structure destabilizes the closed lid configuration. In the absence of a closed lid to isolate the active site from bulk solvent, the PBGS-catalyzed reaction cannot proceed until the external pH is above the pK_a of the amino groups that participate in Schiff base formation. Hence, the hexameric structure exhibits activity with a highly basic optimum pH. Further work is required to test this hypothesis.

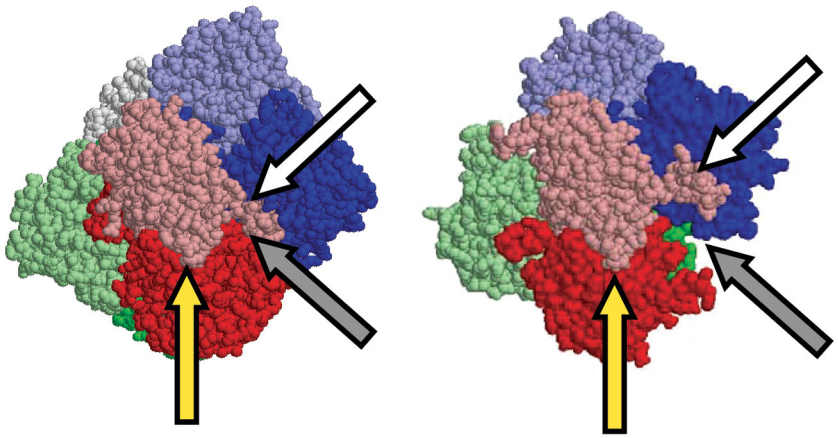

Figure 4 The allosteric magnesium-binding site of PBGS is not present in the hexamer. The arrows indicate subunit interfaces of the human PBGS octamer (left) relative to the hexamer (right). In this representation each dimer is colored with light and dark shades of one of the four colors red, blue, green, and gray. The interfaces shown by the yellow and white arrows are present in the two quaternary forms. The interface shown by the gray arrow, which corresponds to the site of binding the allosteric magnesium, missing from the hexameric form of PBGS.

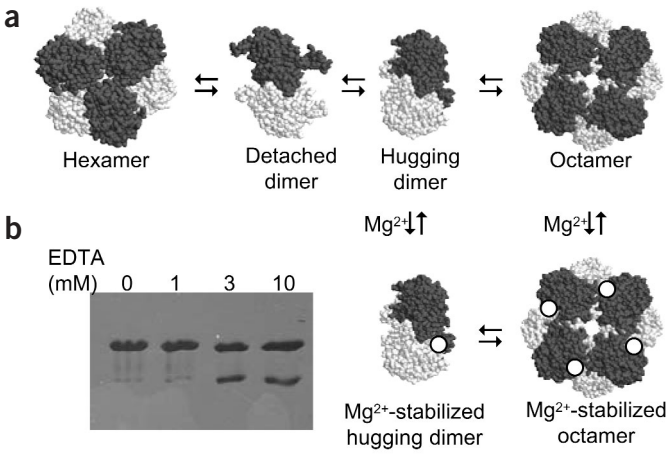

Figure 5 A proposal for the physiologically relevant interconversion of hexameric and octameric PBGS in many species whose PBGS contain the binding determinants for the allosteric magnesium. (**a**) The hexamer can dissociate into detached dimers in a protein concentration–dependent fashion. N-terminal arm movement is required for the formation of the hugging dimer, which can then associate to octamer in a protein concentration–dependent fashion. Binding of the allosteric magnesium stabilizes the hugging dimer and/or octameric structures. Sequence data available to date indicate that the allosteric magnesium is found in PBGS from all photosynthetic eukaryotes, all archaea and all bacterial species except from the genus *Rhodobacter*[24]. The allosteric magnesium is not present in PBGS from metazoa or fungi[24], in which an invariant arginine residue provides a coincident positive charge. (**b**) Native gel electrophoresis of pea PBGS[22], which is isolated in the presence of magnesium, under assay conditions. Present in the samples are 5 mM Mg^{2+}, 10 mM 2-mercaptoethanol, 10 mM ALA and EDTA at 0, 1, 3 and 10 mM. The K_d for binding the allosteric magnesium has been estimated to be 2.5 mM (ref. 22).

Allosteric regulation of PBGS

Despite the fact that the existing structures do not fully explain the mechanism for formation of hexameric PBGS, nor do they definitively establish the structural basis for the kinetic differences between octameric and hexameric PBGS, the current results provide a new approach to understanding the regulation of PBGS function. As described below, the insight provided from identification of a PBGS hexamer has considerable consequence for rethinking the allosteric regulation of PBGS activity in nonhuman species.

Comparison of the PBGS octamer and hexamer reveals a basis for allosteric regulation of PBGS. Despite the fact that all the obvious components of the PBGS active site are contained in the monomer, most PBGS proteins contain a binding site for an allosteric magnesium that is located at the arm-to-barrel interface of the hugging dimer[14,24]. The position of the allosteric magnesium is seen in the crystal structures of both *Pseudomonas aeruginosa*[14] and *Escherichia coli* PBGS[16]. The structures of yeast and human PBGS show that the guanidinium group of an arginine resides in the place of the allosteric magnesium as illustrated previously[2]. If one presumes that all PBGS can exist in the hexameric state under appropriate conditions, then the position of the allosteric magnesium is pertinent to a hexamer-octamer transition because this metal-binding site is present in the octamer (made up of hugging dimers) and absent in the hexamer (made up of detached dimers) (**Fig. 4**). Consistent with the notion that the allosteric magnesium influences a hexamer-octamer equilibrium is the effect of magnesium on the kinetic parameters of *E. coli* PBGS. In this case, the addition of the allosteric magnesium causes the K_m value to decrease from ~2 mM to ~200 μM (ref. 8), which is remarkably reminiscent of the difference between the K_m values of the hexameric and octameric forms of human PBGS (**Table 1**). Also of note is our earlier observation that homogeneously pure *E. coli* PBGS shows multiple bands during native gel electrophoresis, that the mobility of these bands is consistent with the molecular size of octamer, hexamer and dimer, and that addition of magnesium favors the largest (octameric) form[8]. The hexamer-octamer transition defines a new mechanism for metal ion–dependent allosteric regulation of protein function.

Protein concentration–dependent specific activity

We propose that interconversion of PBGS between hexamer and octamer is the mechanism responsible for the protein concentration–dependent specific activity of PBGS from some species. To date we have characterized four different PBGS that contain the allosteric magnesium. The enzymes are from the species *E. coli* (a γ-proteobacter), *Bradyrhizobium japonicum* (an α-proteobacter), *P. aeruginosa* (a γ-proteobacter), and *Pisum sativum* (a green plant). The last three are different from human PBGS in that they do not use an active-site catalytic zinc[24] and they also share the unusual property of protein concentration–dependent specific activity[9,22,25]. The latter property

Table 2 Data collection and refinement statistics

Data collection	
Unit cell (Å)	
$a = b$	89.6
c	153.2
Space group	$P6_3$
Number of independent molecules	2
Number of frames	525
Oscillation angle (°)	0.5
Resolution (Å)	45.0–2.2
Unique reflections	33,615
Completeness (%)	95.7
$I / \sigma(I)$	27.7
R_{sym}[a]	0.05
Refinement	
R_{work}[b]	0.199
R_{free}[c]	0.286
R.m.s. deviations	
Bonds (Å)	0.018
Angles (°)	2.0
Ramachandran plot statistics	
Allowed (%)	90.2
Additionally allowed (%)	9.4
Generously allowed (%)	0.4
Disallowed (%)	0.0
Residues or atoms in the final model	
Molecule A	11–82, 97–124, 140–169, 172–212, 222–330
Product intermediate	1
Molecule B	3–82, 97–122, 140–169, 172–212, 226–328
Zn atoms	2
Water molecules	241

[a] $R_{sym} = E_{hkl}|E_{I\,hkl,i} - \langle I\rangle_{hkl}|/E_{hkl}|\langle I\rangle_{hkl}|$ where $I_{hkl,i}$ is the ith measurement of intensity I_{hkl}. [b] $R_{work} = E_{hkl}|F_{o\,hkl} - F_{c\,hkl}|/E_{hkl}|F_{o\,hkl}|$ where F_o and F_c are observed and calculated structure factors. [c] R_{free} is the same as R_{work} but calculated only for a group of randomly chosen reflections (10% in our case), excluded from the refinement and used only for cross-validation.

indicates that a maximally active oligomer can dissociate into less active or inactive smaller forms. Published mathematical models had considered maximally active octamers dissociating into less active or inactive tetramers and/or dimers[9,22].

The hexameric structure of human PBGS variant F12L leads us to propose that the protein concentration dependence of plant and certain bacterial PBGS is rather due to an equilibrium between a less active hexameric form and a more active octameric form (**Fig. 5a**). The existence of such an equilibrium is supported by sedimentation equilibrium studies on pea PBGS (A.S.W., R.F., and E.K.J., unpublished data). Because magnesium is integral to the difference between the hugging dimer and the alternative detached dimer, binding of this ion is proposed to stabilize the hugging dimer and, hence, the octamer. Removal of magnesium from pea PBGS destabilizes the largest form in favor of a smaller form, where the mobility of the two forms is consistent with that of octamer and hexamer (**Fig. 5b**). In the model, the hexamer is a putative storage form of the PBGS protein because it is less active at physiological pH and is characterized by a K_m value that is well above the physiological concentration of ALA. By contrast, the octamer is active at physiological pH and has a K_m value that is in the proper range of ALA concentrations during active tetrapyrrole biosynthesis.

Together, these studies support the notion that there is a role for PBGS in the complex control of chlorophyll biosynthesis[26–28]. We note that one documented occurrence during the greening of plants is a marked increase in magnesium concentration in the chloroplast[29]. One can imagine that an inactive hexameric storage form allows rapid activation of PBGS as part of a cascade of biochemical changes that accompanies the greening process. It is notable that several gel filtration studies on the quaternary structure of plant and algae PBGS concluded that the oligomer was a hexamer[30]. Literature support for the existence of interconvertible quaternary forms of PBGS separable by anion-exchange chromatography can be found in an early report on PBGS from *Chlorella regularis*[31]. Future crystallographic studies will be needed to prove the existence of hexameric PBGS from plants and bacteria.

METHODS

Genes and constructs. The parent human PBGS is the well characterized N59/C162A[6]. N59 is the more soluble of two codominant alleles encoding PBGS. The C162A mutation removes the possibility of a slowly forming aberrant disulfide bond. The artificial gene for N59/C162A is called WT below. The sense-strand primer used for the QuikChange mutagenesis of WT to the F12L variant was GGCTACCTCCACCCACTGCTTCGGGCC. Several constructs were prepared for the coexpression of WT and the F12L variant in *E. coli*. The order of the genes and the number of promoters did not affect the outcome. The construct containing WT and the F12L variant with one promoter is described. Plasmid DNA containing WT (pET3aWT) and pET17b vector DNA were both digested with *Bam*HI and *Nde*I. The resulting fragments were ligated and transformed into *E. coli* XL1blue, and the resulting plasmid DNA (pET17bWT) was prepared and linearized with *Spe*I and *Bpu*1102I. Plasmid DNA containing the gene encoding the F12L variant (pET3aF12L) was digested with *Xba*I and *Bpu*1102I to produce a fragment containing the gene for the F12L variant. The gene for the F12L variant and the linearized pET17WT vector were ligated such that the ribosomal binding site of the F12L gene was 35 base pairs downstream of the stop codon of WT, and the terminator was 52 base pairs downstream of the stop codon for the F12L gene. Plasmid pET17bWTF12L was transformed into *E. coli* XL1blue and plasmid DNA was prepared and transformed into *E. coli* BLR(DE3) for protein expression as described[6].

Protein purification. The bulk of the protein purification procedure (cell disruption, ammonium sulfate fractionation, hydrophobic chromatography on phenyl-Sepharose, anion-exchange chromatography, and gel-filtration chromatography on Sephacryl S-300) followed the procedures described[6] with the exception that a 70 ml Q-Sepharose column was used for the anion exchange step. The Q-Sepharose buffer was 30 mM potassium phosphate, pH 7.0, 10 mM 2-mercaptoethanol, 10 μM $ZnCl_2$, and used a KCl gradient (**Fig. 3a**).

Kinetic characterization of PBGS variants. Assay buffer was 0.1 M bis-tris propane, 10 mM 2-mercaptoethanol, 10 μM $ZnCl_2$. The reported pH reflects the assay pH after the addition of 10 mM ALA-HCl. For K_m and V_{max} determinations, concentrations of ALA were 10 μM, 30 μM, 100 μM, 300 μM, 1 mM, 3 mM and 10 mM, done in duplicate. ALA-HCl concentration was varied by diluting 0.1 M stock into 0.1 M HCl. Fixed time assays were at 37 °C and used Ehrlich's reagent to determine porphobilinogen formed.

Analytical ultracentrifugation. Protein samples were dialyzed into 30 mM potassium phosphate, pH 7.5, 0.1 mM DTT, and 10 μM $ZnCl_2$. Loading concentrations were 10.6 μM and 12.8 μM for wild type and the F12L variant, respectively. Sedimentation-equilibrium experiments were carried out at 4 °C using a Beckman Optima XL-A analytical ultracentrifuge as described[32]. Temperature-corrected partial specific volumes and solution density calculations used the Sednterp program[33]; the solution density was 1.00191 g ml^{-1} and the partial specific volumes were 0.7394 and 0.7397 ml g^{-1} for the wild-type and mutant proteins, respectively. Data analysis used the HID program (Analytical Ultracentrifugation Facility at the University of Connecticut, Storrs, Connecticut). Model analysis of the data ruled out a single species as the residuals from the fits were nonrandom.

Crystal structure determination. The F12L variant was dialyzed against 50 mM bis-tris propane, 10 mM βME, and 10 μM $ZnCl_2$. Crystals were formed using the sitting drop method; equal volume of the F12L variant (4.0 mg ml^{-1}) was mixed with the precipitant (0.4 M monoammonium hydrogen phosphate). ALA was added equimolar to the protein subunit concentration and crystals formed in 3–5 d. Diffraction data were collected at 100 K on MAR345 image plate detector coupled with RU-200 rotating anode generator equipped with OSMIC optics and operated at 50 kV and 100 mA. Crystals were cryoprotected before freezing by transferring them to reservoir solutions containing 12%, 17%, 23% and 30% (v/v) glycerol for 3 min in each solution. The F12L variant was soaked in 2 mM ALA, which was added to the first two cryoprotectant solutions and 0.2 mM $ZnCl_2$, which was added to the last two solutions in addition to ALA. Diffraction data (**Table 2**) were reduced with the program package HKL2000 (ref. 34).

The structure was solved by molecular replacement with the program package AmoRe[35] by using molecule A of human PBGS structure (PDB entry 1E51) as an initial model. Refinement was carried out with program CNS[36]. Two atoms of Zn appear to have low occupancies.

Coordinates. The coordinates and structure factors have been deposited in the Protein Data Bank (accession code 1PV8).

ACKNOWLEDGMENTS

We thank J. Tannir (Fox Chase Cancer Center (FCCC)), S. Seeholzer (FCCC), T. Guszczynski (US National Cancer Institute (NCI)) and T. Copland (NCI) for technical support. The FCCC DNA synthesis facility, DNA sequencing facility and Research Secretarial Services were used in the preparation of this manuscript. This work was supported by the US National Institute of Environmental Health Sciences, the NCI, and by an appropriation from the Commonwealth of Pennsylvania.

COMPETING INTERESTS STATEMENT

The authors declare that they have no competing financial interests.

Received 14 March; accepted 15 July 2003
Published online at http://www.nature.com/naturestructuralbiology/

1. Battersby, A.R. Tetrapyrroles: the pigments of life. *Nat. Prod. Rep.* **17**, 507–526 (2000).
2. Jaffe, E.K. The porphobilinogen synthase family of metalloenzymes. *Acta Crystallogr. D* **56**, 115–128 (2000).
3. Akagi, R., Yasui, Y., Harper, P. & Sassa, S. A novel mutation of delta-aminolaevulinate dehydratase in a healthy child with 12% erythrocyte enzyme activity. *Br. J. Haematol.* **106**, 931–937 (1999).
4. Schulze, A., Frommhold, D., Hoffman, G.F. & Mayatepek, E. Spectrophotometric microassay for delta-aminolevlinate dehydratase in dried-blood spots as confirmation

for hereditary tyrosinemia type I. *Clin. Chem.* **47**, 1424–1429 (2001).
5. Maruno, M. *et al.* Highly heterogeneous nature of delta-aminolevulinate dehydratase (ALAD) deficiencies in ALAD porphyria. *Blood* **97**, 2972–2978 (2001).
6. Jaffe, E.K., Martins, J., Li, J., Kervinen, J. & Dunbrack, R.L. Jr. The molecular mechanism of lead inhibition of human porphobilinogen synthase. *J. Biol. Chem.* **276**, 1531–1537 (2001).
7. Jaffe, E.K. *et al.* An artificial gene for human porphobilinogen synthase allows comparison of an allelic variation implicated in susceptibility to lead poisoning. *J. Biol. Chem.* **275**, 2619–2626 (2000).
8. Jaffe, E.K. *et al.* Characterization of the role of the stimulatory magnesium of *Escherichia coli* porphobilinogen synthase. *Biochemistry* **34**, 244–251 (1995).
9. Petrovich, R.M., Litwin, S. & Jaffe, E.K. *Bradyrhizobium japonicum* porphobilinogen synthase uses two Mg(II) and monovalent cations. *J. Biol. Chem.* **271**, 8692–8699 (1996).
10. Frankenberg, N., Jahn, D. & Jaffe, E.K. *Pseudomonas aeruginosa* contains a novel type V porphobilinogen synthase with no required catalytic metal ions. *Biochemistry* **38**, 13976–13982 (1999).
11. Erskine, P.T. *et al.* X-ray structure of 5-aminolaevulinate dehydratase, a hybrid aldolase. *Nat. Struct. Biol.* **4**, 1025–1031 (1997).
12. Erskine, P.T. *et al.* X-ray structure of 5-aminolevulinic acid dehydratase from *Escherichia coli* complexed with the inhibitor levulinic acid at 2.0 Å resolution. *Biochemistry* **38**, 4266–4276 (1999).
13. Erskine, P.T. *et al.* The Schiff base complex of yeast 5-aminolaevulinic acid dehydratase with laevulinic acid. *Protein Sci.* **8**, 1250–1256 (1999).
14. Frankenberg, N. *et al.* High resolution crystal structure of a Mg^{2+}-dependent porphobilinogen synthase. *J. Mol. Biol.* **289**, 591–602 (1999).
15. Erskine, P.T. *et al.* MAD analyses of yeast 5-aminolaevulinate dehydratase: their use in structure determination and in defining the metal-binding sites. *Acta Crystallogr. D* **56**, 421–430 (2000).
16. Kervinen, J. *et al.* Mechanistic basis for suicide inactivation of porphobilinogen synthase by 4,7-dioxosebacic acid, an inhibitor that shows dramatic species selectivity. *Biochemistry* **40**, 8227–8236 (2001).
17. Erskine, P.T. *et al.* The X-ray structure of yeast 5-aminolaevulinic acid dehydratase complexed with two diacid inhibitors. *FEBS Lett.* **503**, 196–200 (2001).
18. Erskine, P.T. *et al.* The X-ray structure of yeast 5-aminolaevulinic acid dehydratase complexed with substrate and three inhibitors. *J. Mol. Biol.* **312**, 133–141 (2001).
19. Jaffe, E.K. *et al.* Species-specific inhibition of porphobilinogen synthase by 4-oxosebacic acid. *J. Biol. Chem.* **277**, 19792–19799 (2002).
20. Frere, F. *et al.* Structure of porphobilinogen synthase from *Pseudomonas aeruginosa* in complex with 5-fluorolevulinic acid suggests a double Schiff base mechanism. *J. Mol. Biol.* **320**, 327–247 (2002).
21. Murzin, A.G., Brenner, S.E., Hubbard, T. & Chothia, C. SCOP: a structural classification of proteins database for the investigation of sequences and structures. *J. Mol. Biol.* **247**, 536–540 (1995).
22. Kervinen, J. *et al.* Porphobilinogen synthase from pea: expression from an artificial gene, kinetic characterization, and novel implications for subunit interactions. *Biochemistry* **39**, 9018–9029 (2000).
23. Segel, I.H. *Enzyme Kinetics* 64–71 (Wiley, New York,1975).
24. Jaffe, E.K. An unusual phylogenetic variation in the metal ion binding sites of porphobilinogen synthase. *Chem. Biol.* **10**, 25–34 (2003).
25. Frankenberg, N., Heinz, D.W. & Jahn, D. Production, purification, and characterization of a Mg^{2+}-responsive porphobilinogen synthase from *Psuedomonas aeruginosa*. *Biochemistry* **38**, 13968–13975 (1999).
26. Schneider, H.A. Enzymic capacities for chlorophyll biosynthesis. Activation and *de novo* synthesis of enzymes. *Z. Naturforsch.* **31**, 55–63 (1976).
27. Papenbrock, J., Mock, H.P., Tanaka, R., Kruse, E. & Grimm, B. Role of magnesium chelatase activity in the early steps of the tetrapyrrole biosynthetic pathway. *Plant Physiol.* **122**, 1161–1169 (2000).
28. Papenbrock, J. & Grimm, B. Regulatory network of tetrapyrrole biosynthesis—studies of intracellular signalling involved in metabolic and developmental control of plastids. *Planta* **213**, 667–681 (2001).
29. Walker, D.A. Regulatory mechanisms in photosynthetic carbon metabolism. *Curr. Top. Cell Regul.* **11**, 203–241 (1976).
30. Stolz, M. & Dornemann, D. Purification, metal cofactor, N-terminal sequence and subunit composition of a 5-aminolevulinic acid dehydratase from the unicellular green alga *Scenedesmus obliquus*, mutant C-2A′. *Eur. J. Biochem.* **236**, 600–608 (1996).
31. Tamai, H., Shioi, Y. & Sasa, T. Purification and characterization of δ-aminolevulinic acid dehydratase from *Chlorella regularis*. *Plant Cell Physiol.* **20**, 435–444 (1979).
32. Wu, J.W. *et al.* Crystal structure of a phosphorylated Smad2. Recognition of phosphoserine by the MH2 domain and insights on Smad function in TGF-β signaling. *Mol. Cell* **8**,1277–1289 (2001).
33. Laue, T., Shaw, B.D., Ridgeway, T.M. & Pelletier, S.L. in *Analytical Ultracentrifugation in Biochemistry and Polymer Science* (eds. Harding, S.E., Rowe, A. & Horton, J.C.) 90–125 (Royal Society of Chemistry, Cambridge, UK, 1992).
34. Otwinowski, Z. & Minor, W. Processing of X-ray diffraction data collected in oscillation mode. *Methods Enzymol.* **276**, 307–326 (1997).
35. Navaza, J. An automated package for molecular replacement. *Acta Crystallogr. A* **50**, 157–163 (1994).
36. Jones, T.A., Zou, J.Y., Cowan, S. & Kjeldgaard, M. Improved methods for building protein models in electron density maps and location of errors in these models. *Acta Crystallogr. A* **47**, 110–119 (1991).